

1 Size-resolved identification, characterization and
2 quantification of primary biological organic aerosol
3 at a European rural site

4 *Carlo Bozzetti[†], Kaspar R. Daellenbach[‡], Christoph Hueglin[‡], Paola Fermo[≠], Jean Sciare[†],*
5 *Anneliese Kasper-Giebl[□], Yinon Mazar^{*}, Gülcin Abbaszade[̄], Mario El Kazzi[⊖], Raquel Gonzalez[≠],*
6 *Timor Shuster-Meiseles[□], Mira Flasch^δ, Robert Wolf[†], Adéla Křepelová[†], Francesco*
7 *Canonaco[†], Jurgen Schnelle-Kreis[̄], Jay G. Slowik[†], Ralf Zimmermann[̄][◇], Yinon Rudich^{*}, Urs*
8 *Baltensperger[†], Imad El Haddad^{†*}, and André S. H. Prévôt^{†*}*

9 [†] Laboratory of Atmospheric Chemistry, Paul Scherrer Institute, Villigen 5232, Switzerland

10 [‡] Swiss Federal Laboratories for Materials Science and Technology, EMPA, Dübendorf 8600,
11 Switzerland

12 [≠] Università degli Studi di Milano, Milano 20133, Italy

13 [□] Laboratoire des Sciences du Climat et de l'Environnement, LSCE, CNRS-CEA-UVSQ, Gif-
14 sur-Yvette 91190, France

15 [□] Institute of Chemical Technologies and Analytics, Vienna University of Technology, Wien
16 1060, Austria

17 [□] Department of Earth and Planetary Sciences, Weizmann Institute of Science,
18 Rehovot 76100, Israel

19 □ Helmholtz Zentrum München, German Research Center for Environmental Health (GmbH),
20 Joint Mass Spectrometry Centre, Cooperation Group Comprehensive Molecular Analytics,
21 85764 Neuherberg, Germany

22 □ Electrochemistry Laboratory, Paul Scherrer Institute, Villigen 5232, Switzerland

23 ◇ Analytical Chemistry & Joint Mass Spectrometry Centre, Institute of Chemistry, University of
24 Rostock, 18051 Rostock, Germany

25 E-mail: imad.el-haddad@psi.ch, andre.prevot@psi.ch

26 **Abstract**

27 Primary biological organic aerosols (PBOA) represent a major component of the coarse
28 organic matter (OM_{COARSE} , aerodynamic diameter $>2.5\mu m$). Although this fraction affects human
29 health and climate, its quantification and chemical characterization currently remain elusive. We
30 present the first quantification of the entire $PBOA_{COARSE}$ mass and its main sources by analyzing
31 size-segregated filter samples collected during summer and winter at the rural site of Payerne
32 (Switzerland), representing a continental Europe background environment. The size-segregated
33 water soluble OM was analyzed by a newly developed offline aerosol mass spectrometric
34 technique (AMS). Collected spectra were analyzed by 3-dimensional positive matrix
35 factorization (3D-PMF), showing that PBOA represented the main OM_{COARSE} source during
36 summer and its contribution to PM_{10} was comparable to that of secondary organic aerosol. We
37 found substantial cellulose contributions to OM_{COARSE} , which in combination with gas
38 chromatography mass spectrometry molecular markers quantification, underlined the
39 predominance of plant debris. Quantitative polymerase chain reaction (qPCR) analysis instead

40 revealed that the sum of bacterial and fungal spores mass represented only a minor OM_{COARSE}
41 fraction (<0.1%). X-ray photoelectron spectroscopic (XPS) analysis of C and N binding energies
42 throughout the size fractions revealed an organic N increase in the PM_{10} compared to PM_1
43 consistent with AMS observations.

44 Introduction

45 Primary biological organic aerosol (PBOA) is a major source of coarse aerosol organic matter
46 (OM). The detection of these particles has been the subject of studies for one and a half
47 centuries.¹⁻³ Studies⁴ have related single PBOA components to adverse health effects,⁵ and
48 revealed their important role as ice and cloud condensation nuclei.⁶⁻¹⁰ Emissions of primary
49 biological particles (PBAP) are estimated to be among the largest contributors of pre-industrial
50 organic aerosols,¹¹ therefore a precise estimate of their sources is also important for the
51 development of accurate climate models.⁴ Nevertheless, PBOA characterization and
52 quantification has received less attention than other types of aerosol sources and processes (e.g.
53 traffic, mineral dust, sulfate, wood combustion and secondary organic aerosol), possibly because
54 of technical limitations hindering the understanding of the sources and composition of this
55 fraction.

56 Traditional analytical techniques for the PBOA characterization include optical microscopy,
57 cultivation of specific viable bacteria, fungi and algae and fluorescence microscopy for the
58 quantification of functionalized or autofluorescent specific components.⁴ More recent approaches
59 are classified into molecular techniques (e.g. chemical tracers determination, nucleic acids
60 extraction and amplification), optical techniques (fluorescent and Raman spectroscopy), and non-
61 optical techniques. Fluorescence techniques are of particular relevance because biological

62 materials contain fluorophores.^{12,13} Non-optical approaches include different types of mass
63 spectrometers; among these, we note the recent use of online-aerosol mass spectrometry (AMS)
64 for the study of the submicron fraction.¹⁴⁻¹⁶

65 Despite the vast literature focusing on the quantification of individual PBOA components, the
66 quantification of the total PBOA mass and the main processes by which this fraction enters the
67 atmosphere remains elusive. As a consequence, the International Panel on Climate Change
68 2013¹⁷ reported the global terrestrial PBOA emission to range between 50 and 1000 Tg/yr,
69 highlighting the large gap in our knowledge about this fraction. Within this fraction, 28 Tg/yr
70 were estimated to comprise fungal spore emissions using arabitol and mannitol as tracers.¹⁸ The
71 use of these compounds as specific fungal spores tracers is still subject of discussion in the
72 scientific community^{19,20} and there is a general indispensable need for the determination of
73 PBOA concentrations and major emission processes through size-resolved field observations
74 against which the global models can be evaluated.

75 In this study, we present the first quantification of the total water-soluble PBOA (WSPBOA)
76 mass using an offline Aerodyne Time-of-Flight Aerosol Mass Spectrometer (ToF-AMS). The
77 analysis was performed on PM₁, PM_{2.5} and PM₁₀ (particulate matter with an aerodynamic
78 diameter < 1, 2.5 and 10 μm) filter samples collected concomitantly at the rural site of Payerne,
79 Switzerland. WSPBOA quantification was achieved by 3-dimensional positive matrix
80 factorization analysis (3D-PMF) of water soluble OA mass spectra, following the recently
81 developed methodology described by Daellenbach.²¹ In comparison with previous PBOA online
82 AMS observations,¹⁴⁻¹⁶ the filter samples water extraction step enabled accessing the
83 WSOM_{COARSE} fraction. For the characterization of the main PBOA sources, the dataset was
84 complemented with an unprecedented combination of measurements, including enzymatic

85 cellulose determination, quantification of bacterial and fungal spore DNA via quantitative
86 polymerase chain reaction (qPCR), and gas chromatography mass spectrometry analysis (GC-
87 MS) of organic molecular markers. In this study, we discuss the quantification of the total PBOA
88 mass via 3D-PMF, the quantification of its major components and their possible usage as PBOA
89 tracers including bacteria and fungal spores measured via qPCR, plant debris estimate from *n*-
90 alkanes measurements, and carbohydrates.

91

92 Material and Methods

93 **Sample collection.** We collected in total 87 24h-integrated aerosol samples (Batch A) on
94 quartz fiber filters at the rural background site of Payerne during June-July 2012 and January-
95 February 2013. Batch A included PM₁, PM_{2.5}, and PM₁₀ samples collected in parallel using three
96 High-Volume samplers (Digitel DA-80H equipped with PM₁, PM_{2.5} and PM₁₀ size-selective
97 inlets) operating at 500 L min⁻¹. In total 45 samples were collected during summer (15 samples
98 per size fraction), and 42 during winter (14 samples per size fraction). Additionally, PM₁₀ filters
99 were collected every fourth day throughout 2013 following the same procedure (Batch B). In the
100 following, the subscript *coarse* will denote for a generic aerosol component, the fraction
101 contained between 2.5 and 10 μm.

102 **Aerosol characterization.** An overview of the auxiliary analytical measurements can be
103 found in Table 1, Table S2, and in the Supplementary Information (SI). In this section only
104 offline-AMS, qPCR, and x-ray photoelectron spectroscopy (XPS) will be discussed in details.

105 **Table 1.** Supporting measurements

Measured variable	Batch A	Batch B
-------------------	---------	---------

PM	Gravimetry	All filters	-
WSOM mass spectral fingerprint	Offline-AMS ²¹	All filters	All filters
EC/OC	Thermal Optical Transmittance using a Sunset Lab Analyzer ²² (EUSAAR2) ²³	All filters	-
ions	Ion Chromatography ²⁴	All filters	-
WSOC	Water extraction Thermal Decomposition ND-IR determination using TOC analyzer (SI)	All filters	-
Cellulose	Cellulose enzymatic conversion to D-glucose and photometric determination ²⁵	32 filters (9 summer PM ₁₀ filters, 4 winter PM ₁₀ , 5 summer PM _{2.5} , 9 summer PM ₁ , and 5 summer PM ₁)	-
molecular markers (Table S2)	In-Situ Derivatization Thermal Desorption Gas Chromatography Time-of-Flight Mass Spectrometry (IDTD-GC-MS) ²⁶	40 samples (15 summer PM ₁ , 15 summer PM ₁₀ , 5 winter PM ₁ , 5 winter PM ₁₀)	-
C1s, N1s Binding energies	X-Ray Photoelectron Spectroscopy	6 samples (3 summer PM ₁₀ , 3 summer PM ₁)	-
bacterial and fungal spore DNA	Quantitative Polymerase Chain Reaction genetic analysis ^{27,28}	58 samples (all summer PM ₁ , PM _{2.5} , and PM ₁₀ , all winter PM ₁ and PM ₁₀)	-
Carbohydrates (Table S2)	IC coupled to a Pulsed Amperometric Detector (IC-PAD) ²⁹	All samples	-

106

107 *Offline-AMS*. The Offline-AMS analysis entails an extraction of two 16 mm diameter punches
108 per sample in 10 mL of ultrapure water (18.2 MΩcm, Total Organic Carbon < 5 ppb) via ultra-
109 sonication for 20 min at 30°C. Liquid extracts were subsequently homogenized for 40 s using a

110 vortex mixer and then filtered through 0.45 μm nylon membrane syringe filters. Filtered extracts
111 were aerosolized and the generated particles were dried using a silica gel diffusion drier before
112 measurement by HR-ToF-AMS.³⁰ On average 10 mass spectra (60 s each) of the bulk WSOM
113 were collected per extract. Before each sample measurement, 5 blank mass spectra were
114 collected by nebulizing ultrapure water, and their average was subtracted from the corresponding
115 individual sample mass spectra. The signal of field blank samples measured following the same
116 procedure was statistically not different from the ultrapure water mass spectra.

117 *XPS*. XPS analysis enabled monitoring the binding energies (BE) of C, S and N, providing
118 insight into their oxidation state (typically higher BE are related to higher oxidation numbers),
119 and thereby quantifying the organic N (N_{org}) mass through the size fractions. The same analysis
120 was conducted on 3 field blanks and on N-containing surrogate standards deposited on blank
121 quartz fiber filters. Tested standards included NaNO_3 and $(\text{NH}_4)_2\text{SO}_4$ for the characterization of
122 the most abundant forms of inorganic N, while horseradish peroxidase and chloroperoxidase
123 from *caldariomyces fumago* were used as surrogates for amine and amide containing proteins in
124 PBOA. Signal identification and integration proceeded as follows. The obtained spectra were
125 first aligned with a two-point BE calibration using the Si_{2p} and the O_{1s} peaks deriving from the
126 quartz fiber filters as reference points. We estimated an energy accuracy of 0.3 eV, and an
127 average fitting error of 1.4% by fitting the signals of replicate measurements of standard
128 compounds and blanks and assuming a single Gaussian peak for each atom,. These parameters
129 were then used for the fitting of the blank-subtracted C_{1s} , and N_{1s} signals in environmental
130 samples, which consisted of several peaks from different chemical components. The number of
131 these peaks was determined such that fitting residuals (fraction of signal) equaled the fitting
132 errors determined from the fitting of single compounds. The N_{1s} peak widths were constrained to

133 be equal to the one derived from $(\text{NH}_4)_2\text{SO}_4$ standard, while the $\text{C}_{1\text{s}}$ peak width was determined
134 from blank filters. From the analysis of standard $(\text{NH}_4)_2\text{SO}_4$ we derived an average $\text{N}_{1\text{s}}/\text{S}_{2\text{p}}$ ratio
135 of 0.80 ± 0.02 , which was used to estimate the $\text{N}_{1\text{s}}$ contribution from $(\text{NH}_4)_2\text{SO}_4$ ($\text{N}_{1\text{s}(\text{NH}_4)_2\text{SO}_4}$).
136 This contribution was fixed in proportion of that of $\text{S}_{2\text{p}}$ using the aforementioned $\text{N}_{1\text{s}}/\text{S}_{2\text{p}}$ ratio
137 and $\text{N}_{1\text{s}}$ peak width. This estimate neglected the contribution from organic or non- $(\text{NH}_4)_2\text{SO}_4$
138 sulfate. The uncertainty on the $\text{N}_{1\text{s}(\text{NH}_4)_2\text{SO}_4}$ area was estimated based on the integration of the
139 $\text{S}_{2\text{p}}$ peak. $\text{N}_{1\text{s}}$ fitting sensitivity analysis was performed by varying the $\text{N}_{1\text{s}(\text{NH}_4)_2\text{SO}_4}$ peak position
140 and area within our uncertainties. Only fittings of $\text{N}_{1\text{s}(\text{NH}_4)_2\text{SO}_4}$ with residuals lower than our
141 errors were retained.

142 *qPCR*. We performed a qPCR analysis in order to quantify total bacterial and fungal spore DNA.
143 DNA extraction was conducted following the procedure presented in the SI and specific
144 universal primers (Table S3) were selected for total DNA quantification of bacterial and fungal
145 spores. The extracted DNA was amplified using the qPCR technique described in Lang-
146 Yona.^{27,28} The total number of bacterial cells and fungal spores was estimated assuming a DNA
147 content of $4.74 \cdot 10^{-3}$ pg per bacterial cell and $3 \cdot 10^{-2}$ pg per fungal spore respectively, based on the
148 *Escherichia coli* and *Aspergillus fumigatus* genome lengths (4,639,221 bp and 29,384,958 bp,
149 respectively).³¹ Total bacterial mass was estimated for PM_1 and PM_{10} samples assuming as a
150 reference the dry and wet *E. coli* cell weights ($3 \cdot 10^{-13}$ and $1 \cdot 10^{-12}$ g, respectively),³² while total
151 fungal spores mass was based on the *A. fumigatus* spore weight of $2.9 \cdot 10^{-12}$ g.³³

152

153 3D-PMF

154 OA mass spectra collected by offline-AMS were analyzed using 3D-PMF to apportion the time-
155 dependent size-segregated (PM_1 , $\text{PM}_{2.5}$, PM_{10}) contributions of the water soluble organic

156 sources.³⁴ We adopted a vector-matrix approach,³⁵ also known as “Tucker1” approach³⁶ in which
157 we assumed constant mass spectra throughout the size fractions. The 3D-PMF algorithm
158 describes the variability of the multivariate data-matrix (x) as the linear combination of static
159 factor profiles (f) and their corresponding time and size-dependent contributions (g), such that

$$160 \quad x_{i,j,k} = \sum_{z=1}^p g_{i,j,z} \cdot f_{z,k} + e_{i,j,k} \quad (1)$$

161 Here, $x_{i,j,k}$ denotes an element of the data matrix, while subscripts i , j and k represent time,
162 size and organic ions (250 fitted organic ions in the range m/z 12 to 115) respectively. The
163 subscripts p and z indicate the total number of factors selected by the user, and a discrete factor
164 number ($1 \leq z \leq p$) respectively, while $e_{i,j,k}$ represents an element of the residual matrix.

165 PMF was solved using the multi-linear engine algorithm (ME-2)^{37,38} (using the source finder,
166 SoFi³⁸) which enabled an efficient exploration of the rotational ambiguity by directing the
167 solution toward environmentally relevant rotations. This was achieved by a-priori constraining
168 $f_{z,k}$ and/or $g_{i,j,z}$ elements, and allowing the constrained elements to vary within a predetermined
169 range defined by a scalar a , such that the returned $f_{z,k}'$ or $g_{i,j,z}'$ values satisfy eq 2.

$$170 \quad f_{z,k}' = f_{z,k} \pm a \square f_{z,k} \quad (2)$$

171 Here we constrained the f matrix elements for only one factor, related to hydrocarbon-like
172 organic aerosol (HOA) from traffic³⁹ (SI).

173 PMF data and error input matrices (x and s) were constructed including ten mass spectral
174 repetitions per filter sample. Data and error matrices were rescaled to $WSOM_i$ in order to
175 compare source apportionment results with external tracers. $WSOM_i$ concentrations were
176 estimated from the $WSOC_i$ measurements multiplied by the OM/OC_i ratios determined from
177 offline-AMS HR analysis (measured OM/OC_i distribution 1st quartile 1.89, 3rd quartile 2.01).⁴⁰ In

178 total, the 3D-PMF input matrices comprised 87 samples corresponding to 29 filters per size
179 fractions.

180 The error matrix elements $s_{i,j,k}$ were determined according to eq 3 by propagating the blank
181 standard deviation $\sigma_{i,j,k}$ and the signal error $\square_{i,j,k}$ accounting for electronic noise, ion-to-ion
182 variability at the detector, and ion counting statistics.^{41,42}

$$183 \quad s_{i,j,k} = \sqrt{\square_{i,j,k}^2 + \square_{i,j,k}^2} \quad (3)$$

184 The optimization of the 3D-PMF results is thoroughly presented in the SI. Briefly, to improve
185 the factor separation we up-weighted selected variables dividing their corresponding
186 uncertainties by a scalar c (>1).⁴³ The sensitivity of model outputs to c and a -values was assessed
187 and only solutions matching selected criteria were retained (SI). The variability of the results
188 amongst the selected solutions was considered our best estimate of model errors.

189 PMF factor contributions to total OM were estimated after PMF analysis as:

$$190 \quad ZOA_i = \frac{WSZOA_i}{R_z} \quad (4)$$

191 Here, $[WSZOA]$ and $[ZOA]$ denote for a generic Z source the concentration of the ambient water
192 soluble organic aerosol and the total organic aerosol respectively, while R_z indicates the recovery
193 efficiency for that source. In total, 5 OA factors were separated including HOA, summer
194 oxygenated OA (S-OOA), winter oxygenated OA (W-OOA), biomass burning OA (BBOA), and
195 primary biological OA (PBOA). The $R_{z,med}$ determined by Daellenbach²¹ were applied to all
196 factors except for PBOA, whose recovery was not previously estimated. Accordingly, we shall
197 report hereafter the concentration of WSPBOA and estimate the PBOA water solubility.

198 Source apportionment errors ($\sigma_{S.A.,Z,i}$) were estimated according to eq 5, which accounts for R_Z
199 and rotational uncertainty ($\sigma_{PMF,RZ,i}$), measurement repeatability ($\sigma_{REP,i}$), and WSOM uncertainty
200 ($\sigma_{WSOC,i}$).

201
$$\sigma_{S.A.,Z,i} = \sqrt{\sigma_{PMF,RZ,i}^2 + \sigma_{REP,Z,i}^2 + f_{Z,i}^2 \cdot \sigma_{WSOM,i}^2}$$
 (5)

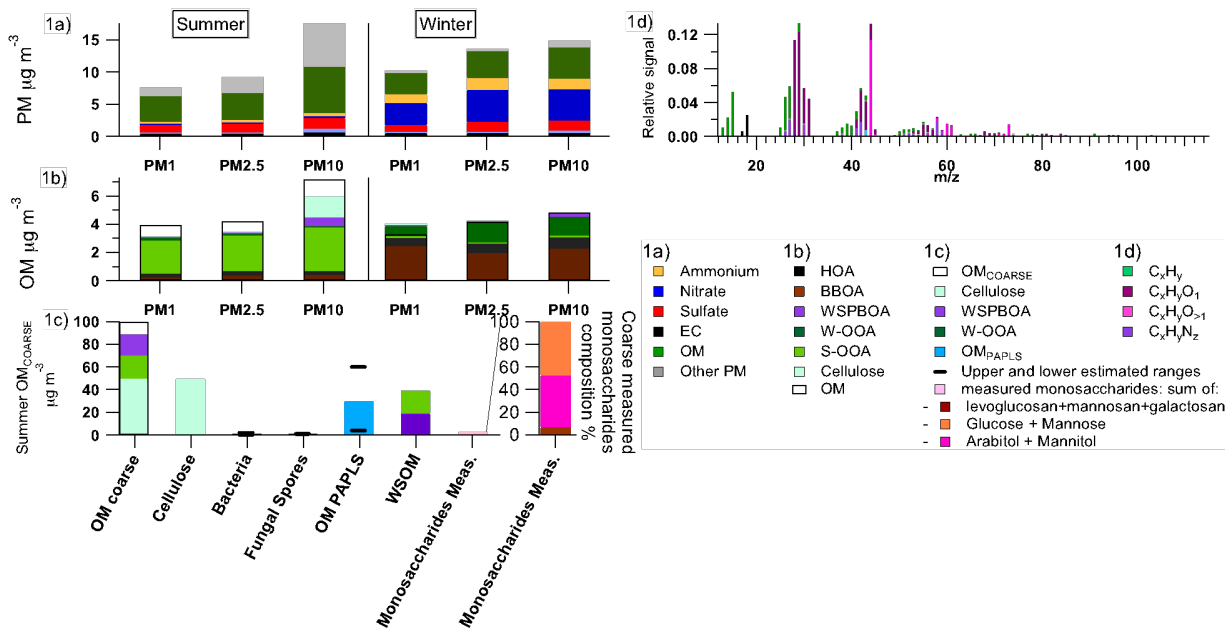
202 Here f_Z denotes the relative contribution of the generic factor Z to WSOM. $\sigma_{WSOM,i}$ includes
 203 WSOC blank variability and measurement repeatability. The $\sigma_{PMF,RZ,i}$ term includes the
 204 variability of the rescaled PMF solutions and represents our best estimate of recovery errors and
 205 rotational ambiguity. The $\sigma_{REP,Z,i}$ term was considered as our best estimate of experimental
 206 repeatability/errors and represents the variability of PMF results for the measurements
 207 repetitions.

208

209 Results and Discussion

210 PM major components

211 A complete overview of the size-segregated chemical composition of winter and summer PM
 212 components is presented in Figure 1a. In the following, average and median values are indicated
 213 with the subscripts *avg* and *med*, respectively.



214

215 **Figure 1.** 1a) Seasonal PM chemical composition of the different size fractions. The OM_i
216 estimate was calculated from OC_i measurements multiplied by the corresponding OM/OC_i
217 retrieved from offline-AMS HR analysis. 1b) Average seasonal aerosol sources contributions to
218 OM in the different size fractions. White are consistent with our estimate of the water insoluble
219 PBOA fractions (Figure S8). Cellulose in particular represents the 82%_{avg} of water insoluble
220 OM_{COARSE} .
221 1c) Summer OM_{COARSE} major components. 1d) WSPBOA high resolution AMS mass spectrum.
222

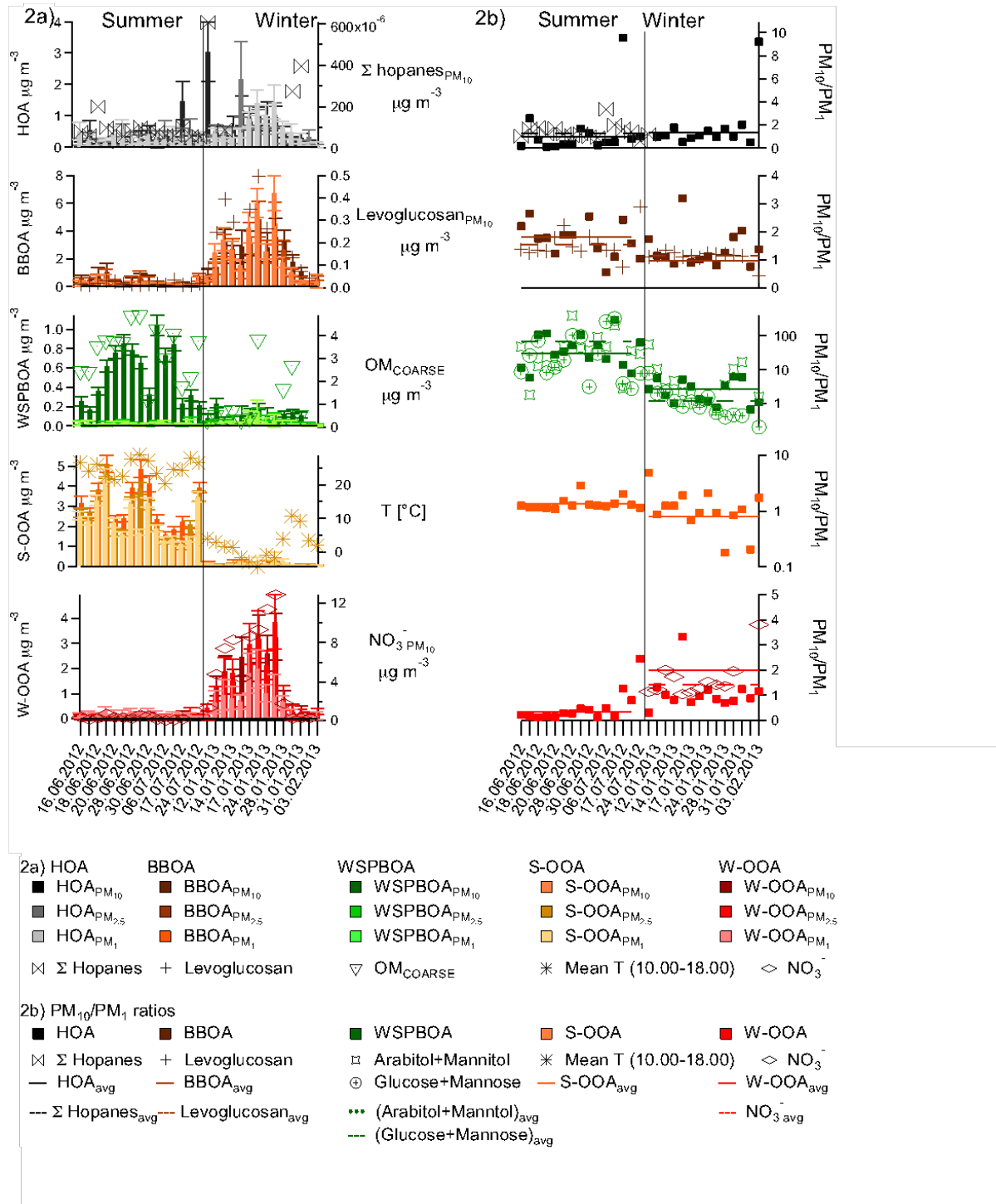
223 OM represented a major component of PM during summer and winter. While during winter
224 large part of the OM_{10} (87%) was comprised in the $PM_{2.5}$ fraction, during summer this fraction
225 represented only 58%. In contrast, during summer secondary inorganic species (SO_4^{2-} , NH_4^+ , and
226 NO_3^-) did not manifest a comparable increase in PM_{COARSE} (85% of the mass comprised in the
227 $PM_{2.5}$ fraction) suggesting a small contribution of additional secondary aerosols in the coarse
228 fraction. Overall OM_{COARSE} accounted for $3 \mu g m^{-3}_{avg}$ during summer, and as will be shown in
229 the following, large part of this fraction constituted of PBOA (Figure S13).

230 Similarly to OM, dust likely from resuspension⁴⁴ was enhanced in the coarse fraction
231 especially during summer. The upper limit for the inorganic $dust_{COARSE}$ concentration was
232 estimated as the difference between inorganic PM_{10} and inorganic $PM_{2.5}$ ($PM_{COARSE,inorg}$), and
233 accounted for 31%_{avg} during summer and 5%_{avg} during winter, although this estimate can include
234 small sea salt contributions (SI). The obtained $(Ca^{2+}/PM)_{COARSE,inorg}$ value of 4.2%_{med} (1st quartile
235 3.2%, 3rd quartile 7.7%) was consistent with the ratios reported by Chow⁴⁵ for 20 different dust
236 profiles ($3.5 \pm 0.5\%$), and with values reported by Amato in Zürich.⁴⁶ As a comparison, the total
237 OM_{COARSE} concentration represented 36%_{avg} of PM_{COARSE} ($8.4 \mu g m^{-3}$), compared to the 62%_{avg}
238 for $dust_{COARSE,inorg}$.

239

240 **Size resolved OA source apportionment**

241 In this section we present the validation of the 3D-PMF factors (HOA, BBOA, W-OOA, S-OOA,
 242 and WSPBOA) which enabled the quantification of WSPBOA. Average source apportionment
 243 results are presented in Figure 1b and Figure 2.



244

245 **Figure 2.** 3D-PMF source apportionment results. 2a) Size fractional time series of PMF factors,
246 corresponding tracers, and temperature. Error bars represent source apportionment uncertainty.
247 2b) Size fractional increase (PM_{10}/PM_1) time series of PMF factors, and corresponding tracers.
248

249 3D-PMF factors were associated to aerosol sources or processes according to mass spectral
250 features, seasonal contributions, size fractional contributions, and correlation with tracers (Figure
251 2). Given the lack of widely accepted methodologies to estimate the uncertainty of PMF results,
252 in this work we considered $\sigma_{S.A.,k,i}$ (Methodology section) as our source apportionment
253 uncertainty, while the statistical significance of the factor contributions for each size fraction was
254 based on our best error estimation ($\sigma_{S.A.,k,i}$, Table S4).

255 HOA and BBOA contributions represented the only anthropogenic primary sources resolved in
256 Payerne. In particular, HOA correlated with hopanes present in lubricant oils with a $R=0.54$ (SI).
257 This correlation is also supported by the summer $(HOA/EC)_{med}$ ratio (0.63_{med}) being consistent
258 with other European studies reported by El Haddad and references therein.⁴⁷ BBOA instead
259 correlated with levoglucosan produced by cellulose pyrolysis ($R=0.94$). A levoglucosan/BBOC
260 ratio of 0.18_{med} was found, consistent with values reported (Huang and references therein⁴⁸) for
261 ambient BBOA observations. Both HOA and BBOA showed statistically significant
262 contributions ($>3\sigma$) only in the submicron fractions. The seasonal trend of these anthropogenic
263 factors was also significantly different: while the HOA (traffic) contribution was relatively stable
264 and small across the year, BBOA showed a strong seasonality, rising from $6\%_{avg}$ of OM_1 during
265 summer to $73\%_{avg}$ during winter.

266 Two OOA factors characterized by high CO_2^+ contributions were separated according to their
267 different seasonal trends. While W-OOA showed a strong correlation with NO_3^- ($R=0.94$), S-
268 OOA showed a positive non-linear correlation with temperature, following the behavior of
269 biogenic volatile organic compounds emissions.⁴⁹ The relative contribution of W-OOA to OM_1

270 rose from 5%_{avg} during summer to 22%_{avg} during winter, while the S-OOA contribution to OM₁
271 decreased from 59%_{avg} during summer to 4%_{avg} during winter. W-OOA was the only factor
272 significantly contributing (within 3 σ) to OM in the size range 1-2.5 μm (48%_{avg} of the W-OOA
273 mass in winter), while the W-OOA_{COARSE} contribution was never statistically significant.
274 NH₄NO₃ behaved similarly with 31%_{avg} of the mass in winter comprised in PM_{2.5}-PM₁. During
275 summer instead S-OOA showed a different behavior in the three size fractions: its contribution
276 was significant for PM₁, but not in the size range 1-2.5 μm . The overall S-OOA_{2.5} fraction
277 accounted for 82 \pm 2%_{avg} of the mass, while the remaining 18 \pm 2%_{avg} was included in OM_{COARSE}.
278 Considering the sum of both OOA factors, the OOA/NH₄⁺_{med} ratio for PM₁ was 2.1, consistent
279 with values reported by Crippa⁵⁰ for 25 different European rural stations, suggesting that Payerne
280 can be representative of typical European rural environments.

281 The last PMF factor showed an unusual size fractionation with 96%_{avg} of its mass comprised in
282 the PM_{COARSE} during summer (0.54 \pm 0.02 $\mu\text{g m}^{-3}$), corresponding to 49% of the WSOM_{COARSE}
283 (or 19%_{avg} of the OM_{COARSE}). This factor was ascribed to water soluble primary biological
284 organic aerosol, given its striking mass spectral resemblance to biological carbohydrates and
285 plant debris extracts with high contribution from C₂H₄O₂⁺, C₂H₅O₂⁺ and C₃H₅O₂⁺ (Figure 1d, S3,
286 S10), its enhancement in OM_{COARSE} especially during summer, and its correlations with
287 biological aerosol components such as arabitol, mannitol, glucose,^{19,20,51,52} cellulose, total
288 bacteria, and fungal spores. The detection of such factor was unprecedented in the AMS
289 literature given the limited transmission efficiency of the AMS aerodynamic lens for the coarse
290 fraction⁵³, although Schneider¹⁵ proposed the use of some of the PBOA fragments detected here
291 to assess the contribution of PBOA to PM₁ from online AMS measurements in the Amazon.

292 Also during winter WSPBOA showed a smaller but still significant contribution to the
293 OM_{COARSE} (30% of $WSOM_{COARSE}$ or 8% of OM_{COARSE}) with 68%_{avg} of the mass comprised in the
294 coarse fraction. This result was corroborated by a minor but statistically significant enhancement
295 in the coarse fraction (in comparison with $PM_{2.5}$) of biological carbohydrates
296 (monosaccharides_{BIO}: Σ (glucose, mannose, arabitol and mannitol)), cellulose, and fungal spores.
297 The chemical characteristics and origin of this fraction will be thoroughly discussed in the
298 following sections.

299 Composition of OM_{COARSE} .

300 This section presents a detailed characterization of OM_{COARSE} , of which 91%_{avg} of the mass was
301 ascribed to PBOA.

302 *Water soluble and insoluble OM_{COARSE} .* Figure 1c displays the relative chemical composition of
303 OM_{COARSE} during summer. The major part of OM_{COARSE} could be ascribed to cellulose
304 (50±20%_{avg}) and $WSOM_{COARSE}$ (38%_{avg}). Given the low cellulose water solubility, and
305 consequently its negligible contribution to $WSOM$, the two fractions together accounted for
306 88%_{avg} of the OM_{COARSE} . Regarding the origin of the $WSOM_{COARSE}$ fraction, 3D-PMF results
307 revealed that only WSPBOA and WSS-OOA contributed significantly to $WSOM_{COARSE}$ during
308 summer, explaining respectively 51%_{avg} and 49%_{avg} of the $WSOM_{COARSE}$ mass. Assuming the
309 water insoluble OM_{COARSE} fraction not ascribed to S-OOA to be entirely related to PBOA, we
310 calculated a R_{PBOA} lowest estimate of 0.18_{med} (1st quartile 0.15, 3rd quartile 0.25) according to eq
311 S2, S3 and S4. This assumption was corroborated by the high cellulose contributions to the water
312 insoluble OM_{COARSE} fraction (82%) and by the good correlation of WSPBOA with OM_{COARSE} -S-
313 OOA_{COARSE} ($R=0.54$), especially considering that the water insoluble OM_{COARSE} fraction
314 represented 62%_{avg} of the total OM_{COARSE} .

315 *Contribution of carbohydrates to PBOA and OM_{COARSE}.* Measured carbohydrates
316 (carbohydrates_{meas}: Σ (monosaccharides_{BIO}, mannosan, levoglucosan, and galactosan))
317 represented 3% of OM_{COARSE} (8% of WSOM_{COARSE}), of which 93%_{avg} was related to
318 monosaccharides_{BIO}. This fraction, albeit minor, was highly correlated with PBOA ($R=0.73$) and
319 cellulose ($R=0.85$), showing a size fractionation similar to WSPBOA especially during summer
320 with 96%_{avg} of the mass included in the OM_{COARSE}. A similar behavior was noted in winter, with
321 29%_{avg} of the carbohydrates_{meas,COARSE} consisting of monosaccharides_{BIO}, suggesting a minor, but
322 statistically significant contribution of primary biological emissions, consistent with WSPBOA
323 from 3D-PMF results (figure 2). Also other biological components, such as cellulose and fungal
324 spores showed a small but significant contribution in winter (respectively $0.06 \mu\text{g m}^{-3}$ and 2×10^1
325 spores m^{-3} detected on the 31st of January 2013 PM₁₀ filter sample). However, the overall
326 correlation of single monosaccharides_{BIO} with each other and with other PBOA components was
327 relatively poor, indicating a high variability in the molecular composition of the carbohydrates.
328 Such variability highlighted the diversity of biological processes producing these sugars, clearly
329 hindering their use as single tracers for reliably estimating PBOA concentrations in our
330 conditions.

331 By ascribing all the monosaccharides_{BIO,COARSE} to WSPBOA we estimated a contribution of
332 monosaccharides_{BIO} to WSPBOA of 15%_{avg}. Consistently, the WSPBOA average mass spectrum
333 (Figure 1d), similarly to BBOA, showed a typical fingerprint deriving from carbohydrate
334 fragmentation¹⁵ as evidenced by strong contributions from $\text{C}_2\text{H}_4\text{O}_2^+$, $\text{C}_2\text{H}_5\text{O}_2^+$ and $\text{C}_3\text{H}_5\text{O}_2^+$
335 fragments (Figure 1b, S3, S4, S10). We estimated that >89% of the remaining WSPBOA fraction
336 could be related to water soluble polysaccharides (after the subtraction of the
337 monosaccharides_{BIO} mass spectrum using D-mannitol and D-glucose as surrogates). This

338 estimate was based on the non-monosaccharides_{BIO}-WSPBOA mass spectrum, assuming
339 $C_2H_4O_2^+$, $C_2H_5O_2^+$ and $C_3H_5O_2^+$ as specific carbohydrates fragmentation tracers¹⁵ (Figure S4),
340 and using amylopectin and starch (Figure S10) as surrogates for polysaccharides. This result,
341 together with the high cellulose contribution to OM_{COARSE} , indicated that the majority of PBOA
342 consisted of carbohydrates.

343 Part of the remaining WSPBOA fraction instead was attributed to N_{org} . 3D-PMF results
344 showed that WSPBOA explained great part of the variability of minor N-containing fragments
345 ($C_3H_9N^+$, $C_3H_8N^+$, $C_5H_{12}N^+$), consistent with XPS observations of an increased N_{org} signal in
346 PM_{COARSE} . The WSPBOA spectrum as expected showed a higher N/C ratio (0.061) than other
347 factors. Overall both the carbohydrate signature and the increased N/C content were consistent
348 with the interpretation of our factor as WSPBOA.

349 *Quantification of OM related to particulate abrasion products from leaf surfaces (OM_{PAPLS})*
350 *using n-alkanes.* n-alkanes (C18-C39) measured via gas chromatography mass spectrometry
351 (IDTD-GC-MS) showed distinct signatures during the different seasons and particle sizes. While
352 during winter most of the alkane mass was contained within PM_1 (90% for alkanes with an odd
353 number of C; 97% for alkanes with an even number of C), during summer only 50%_{avg} and
354 70%_{avg} of the odd and even alkanes were contained within PM_1 . The summer-time signatures
355 were consistent with Rogge's⁵⁴ observations of alkane emissions from OM_{PAPLS} dominated by
356 odd alkanes with the highest contributions from hentriacontane (C31) followed by nonacosane
357 (C29) and tritriacontane (C33) (Figure S9). By contrast, in winter we observed a higher
358 contribution of smaller alkanes (C19-C24), without a clear odd/even predominance pattern,
359 which was consistent with winter urban observations⁵⁵ possibly related to temperature-driven
360 partitioning of combustion emissions, and consistent with vehicular fuel combustion profiles.^{47,56}

361 This was corroborated by a slight increase in the average HOA concentration during winter
362 compared to summer (Figure 2). We estimated the contribution of OM_{PAPLS} by applying a
363 chemical mass balance approach (SI) using the *n*-alkanes/OM_{PAPLS} ratios reported by Rogge.^{56,57}
364 Assuming either green or dead leaves, and a possible (OM/OC)_{green,dead leaves} range between 1.2
365 and 2.2, the total estimated range for OM_{PAPLS,COARSE} spanned from 0.5 to 1 µg m⁻³_{avg},
366 corresponding to 16-32%_{avg} of the OM_{COARSE}. This result, together with high cellulose
367 contributions, indicated that plant debris was the dominating source of OM_{COARSE}.

368 *Fungal spores.* Fungal spores measured by qPCR represented a minor component of OM. During
369 summer, their contribution was above the detection limit only in the coarse fraction, representing
370 just 0.01%_{avg} of the OM_{COARSE} mass (corresponding to 0.4 ng m⁻³, or 2·10² spores·m⁻³).
371 Nevertheless, the measured fungal spore/m³ concentration during summer was consistent with
372 ranges reported in other studies.⁵⁸ During winter, only one PM₁₀ sample showed concentrations
373 above the detection limits. The summer arabitol/fungal spore (5·10² pg/spore_{avg}) and
374 mannitol/fungal spore (8·10² pg/spore_{avg}) ratios were noticeably variable and higher than those
375 reported by Bauer¹⁹ (1.2 pg arabitol/fungal spore, 1.7 pg mannitol/fungal spore), suggesting that
376 these compounds are not unique fungal spore tracers, but given the high levels of cellulose and
377 OM_{PAPLS} could be related to plant debris, as already proposed by other studies.²⁰

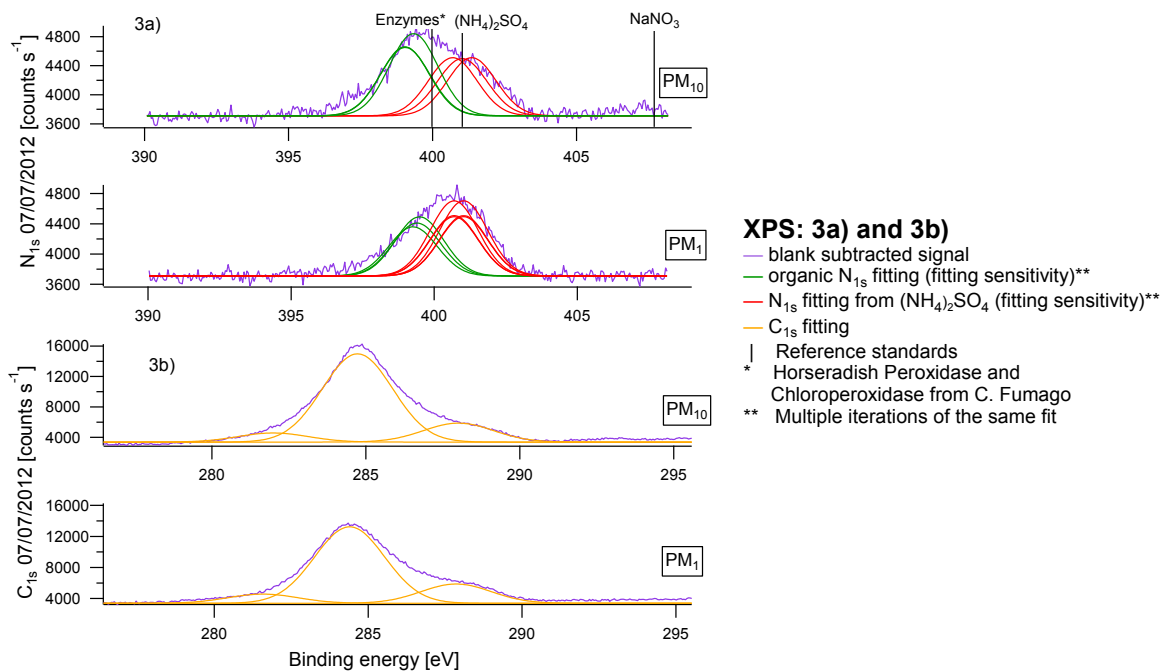
378 *Bacteria.* Likewise, total bacterial mass estimated by qPCR represented a minor contributor to
379 OM_{COARSE}. Assuming dry or wet *E. coli* cellular weights (SI), the total PM₁₀ bacterial mass
380 during summer was estimated as 1.3±0.7 ng m⁻³_{avg} or 4±0.2 ng m⁻³_{avg}, corresponding to 2·10³
381 cells m⁻³_{avg}. This is consistent with the ranges reported in other studies,⁵⁸⁻⁶⁰ especially
382 considering that low concentrations are commonly observed at remote and rural locations.⁶¹ The
383 bacterial size fractionation seasonality was similar to the other biological components: while

384 69%_{avg} of the bacterial mass was comprised between the PM₁₀ and PM₁ fraction during summer,
385 all bacterial mass ($2 \cdot 10^3$ cells m⁻³_{avg}) was detected in the submicron fraction during winter.

386 *Surface chemical composition from XPS analysis.* Another approach to look at the entire
387 aerosol is to study the chemical composition of its surface. This was performed by XPS
388 measurements, which enabled monitoring the evolution of the C_{1s} and N_{1s} BE throughout the
389 different size fractions and thus providing chemical information also about the water insoluble
390 fraction. Although XPS sensitivity was limited to the particle surface (7 nm thickness) and low
391 volatility compounds (XPS technique operates under high vacuum at 10⁻¹⁰ torr), results showed a
392 significant increase of N_{org} in the PM_{COARSE}. We resolved both an inorganic and organic N_{1s}
393 peak, with N_{1s,org} occurring at a lower BE (397.7±0.3 eV, Figure 3a) than that of N<sub>1s(NH₄)₂SO₄
394 and NaNO₃ (400.0±0.8 eV and 407.7±0.4 eV respectively). Likewise, tested N_{org} surrogates
395 (horseradish peroxidase and chloroperoxidase from *caldariomyces fumago*) showed the N_{1s} peak
396 occurring at similar BE (398.7±0.3 eV) corroborating our interpretation of the N_{org} peak position.
397 Overall we observed a substantial increase of the N_{org} signal in PM₁₀ in comparison to PM₁
398 (Figure 3a) reflected by an N_{org}/C_{1s} ratio increase from 0.022±0.001 in PM₁ to 0.027±0.005 in
399 PM₁₀. From the N_{org}/C_{1s} ratio and from the bulk total C measurements (TC=EC+OC)_{Sunset}, we
400 estimated the N_{org,1} and N_{org,10} concentrations to be 0.05±0.03 μg m⁻³_{avg} and 0.13±0.01 μg m⁻³_{avg}
401 respectively. This estimate assumed N_{org} to follow the TC intra-particle concentration gradient.
402 While a crude assumption, this is the best and only methodology providing an estimate of the
403 N_{org} total mass.</sub>

404 Figure 3b displays the C_{1s} peak fitting for a PM₁ and a PM₁₀ filter sample. We report an
405 increase of the less oxidized C_{1s} fraction (C_{1s} peak at lower BE) in PM₁₀, which was qualitatively
406 consistent with the odd-alkanes size fractionation. Overall, in all size fractions, the dominant C_{1s}

407 contribution did not derive from the most oxidized C_{1s} peak (Figure 3b), but from the
 408 intermediate oxidized C peak, which could be related to alcohols, ketones, and aldehydes. This
 409 result, although relative only to the surface and to the less volatile fractions, seemed in
 410 agreement with other studies.⁶²



411
 412 **Figure 3.** 3a) XPS measurements: N_{1s} peak fitting (PM_1 and PM_{10} sample from 04/07/2012). 3b)
 413 XPS measurements: C_{1s} peak fitting (PM_1 and PM_{10} sample from 04/07/2012).

414
 415 **Yearly estimate of PBOA relative contribution to OM_{10}**

416 From 3D-PMF analysis we identified a set of AMS fragments as potential PBOA tracers (figure
 417 S4). Among these fragments we selected $C_2H_4O_2^+$ and $C_2H_5O_2^+$ to estimate the PBOA
 418 contribution for the entire year 2013 (batch B) given their relatively high signal to noise, and
 419 because they are commonly fitted in HR analysis. Both fragments showed a contribution
 420 statistically higher than 0 within 1σ only to the BBOA, PBOA, and HOA factors. However,
 421 given the low HOA concentration at the rural site (Figure 2a), and given the low contribution of

422 the two fragments to the HOA profile (0.02 and 0.03% respectively) we neglected the HOA
 423 contribution to $C_2H_4O_2^+$ and $C_2H_5O_2^+$. Therefore the water soluble $C_2H_5O_2^+$ and $C_2H_4O_2^+$
 424 fractional contribution to WSOM ($WSfC_2H_5O_2^+_i$ and $WSfC_2H_4O_2^+_i$) could be expressed as:

$$425 \quad WSfC_2H_5O_2^+_i = fC_2H_5O_2^+_{WSPBOA} \cdot \frac{WSPBOA}{WSOM}_i + fC_2H_5O_2^+_{WSBBOA} \cdot \frac{WSBBOA}{WSOM}_i \quad (6)$$

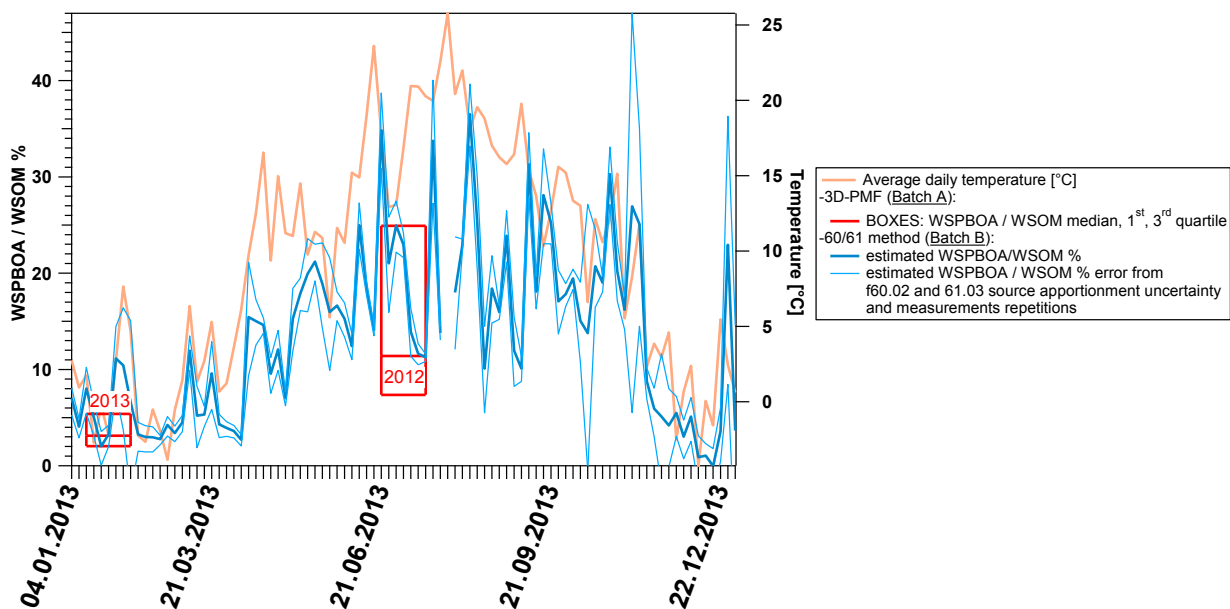
$$426 \quad WSfC_2H_4O_2^+_i = fC_2H_4O_2^+_{WSPBOA} \cdot \frac{WSPBOA}{WSOM}_i + fC_2H_4O_2^+_{WSBBOA} \cdot \frac{WSBBOA}{WSOM}_i \quad (7)$$

427 Where $fC_2H_5O_2^+_{PBOA}$, $fC_2H_4O_2^+_{PBOA}$, $fC_2H_5O_2^+_{BBOA}$, $fC_2H_4O_2^+_{BBOA}$ denote the $C_2H_5O_2^+$, and
 428 $C_2H_4O_2^+$ fractional contributions to the WSPBOA and WSBBOA mass spectra.
 429 $(WSPBOA/WSOM)_i$ values could be derived by solving the two linear equation system. This
 430 approach will be referred to as “60/61 methodology” in the following. We assessed the accuracy
 431 of the 60/61 methodology by comparing the $(WSPBOA/WSOM)_i$ values obtained from 3D-PMF
 432 with the values predicted from the 60/61 methodology for the Batch A PM_{10} filter samples.
 433 During summer the $(WSPBOA/WSOM)_{med,3D-PMF}/(WSPBOA/WSOM)_{med,60/61 \text{ methodology}}$ ratio was
 434 0.98, while during winter 0.85. The winter discrepancy was likely due to non-negligible
 435 contributions of W-OOA or other sources to $fC_2H_4O_2^+$ and $fC_2H_5O_2^+$. However the two
 436 methodologies yielded highly correlated time series ($R^2=0.81$) and agreed within 15%, with
 437 much better agreement during summer.

438 From the 60/61 methodology we estimated a $WSPBOA/WSOM_{avg}$ of 20% in summer, and 6% in
 439 winter. Assuming a R_{PBOA} of 0.18_{med} (SI), the average PBOA contribution to OM_{10} was estimated
 440 as 37%_{avg}, with higher values during summer (60%_{avg} vs. 19%_{avg} in winter).

441 Overall, these results revealed that the contribution of PBOA to OM_{10} , mainly from plant debris,
 442 may be as high as SOA contribution during summer in Payerne. While Payerne can be
 443 considered as representative of typical European rural environments⁵⁰ and therefore results here
 444 may be extended to other sites, other field observations are indeed required. This work represents

445 a benchmark for future field studies providing a methodology for the thorough determination of
446 PBOA mass and origin, and one of the first size-segregated datasets necessary to constrain
447 PBOA in global models.



448
449
450 **Figure 4.** 2013 yearly WSPBOA₁₀ relative contribution to WSOM₁₀ estimated from the 60/61
451 methodology (Batch B). Red boxes denote WSPBOA relative contribution (median, 1st and 3rd
452 quartiles) to WSOM₁₀ during June-July 2012 and January-February 2013 determined by 3D-PMF
453 analysis (Batch A). The uncertainty relative to measurements repetitions and to the
454 apportionment of fC₂H₄O₂⁺ and fC₂H₅O₂⁺ can be interpreted as a precision estimate, while the
455 sensitivity analysis comparing 3D-PMF and 60/61 methodology results, shows an underestimate
456 of the WSPBOA/WSOM ratio calculated with the 60/61 methodology of 2%_{med} during summer
457 and 15%_{med} during winter.

458
459 ASSOCIATED CONTENT

460 Supporting Information. Detailed methodology descriptions of WSOC, qPCR, XPS, and
461 IDTD-GC-ToF-MS measurements; OM_{PAPLS} determination; source apportionment optimization.
462 This material is available free of charge via the Internet at <http://pubs.acs.org>.

463 AUTHOR INFORMATION

464 **Corresponding Author**

465 *Address: OFLA/004, 5232 Villigen PSI, Switzerland; Phone: +41 56 310 4202; e-mail:
466 andre.prevot@psi.ch.

467 * Address: OFLB/002, 5232 Villigen PSI, Switzerland; Phone: +41 56 310 2785; e-mail:
468 imad.el-haddad@psi.ch.

469 **Author Contributions**

470 †C.B. wrote the manuscript. †C.B. and †*I.E.H performed the data analysis and source
471 apportionment. †*A.S.H.P., †*I.E.H., †C.B. and †J.G.S. designed the experiment. †C.B. and †A.K.
472 performed the offline-AMS analysis. *P.F. and *R.G. performed WSOC measurements. □J.S.
473 measured carbohydrates_{meas} and EC/OC. ‡C.H. collected the samples, and measured ions and
474 EC/OC. □G.A., □R.Z., and □J.S.-K. performed IDTD-GC-ToF-MS measurements. □Y.R., T.S.M.
475 and □Y.M. performed qPCR measurements. °M.E.K., C.B. and I.E.H. performed XPS
476 measurements. □A.K.-G. and □M.F. performed cellulose measurements. All authors gave
477 approval to the final version of the manuscript.

478 **Funding Sources**

479 This work was supported by the Federal Office for the Environment in Switzerland

480 ACKNOWLEDGMENT

481 Carlo Bozzetti acknowledges the Lithuanian–Swiss Cooperation Programme “Research and
482 Development” project AEROLIT (Nr. CH-3-MM-01/08). Imad El Haddad acknowledges the
483 Swiss National Science Foundation (project number IZERZO 142146). Yinon Rudich

484 acknowledges support from the Israel Science Foundation, grant #913/12 and from the Dollond
485 Foundation. We acknowledge Saurer, M. and Schmid, L. for providing milled oak leaves, and
486 Goldsmith G. R. for the NCBI BLAST research.

487 REFERENCES

488 (1) Pasteur, L. Mémoire sur les corpuscles organises qui existent dans l'atmosphère. Examen
489 de la doctrine des générations spontanées. *Ann. Sci. Nat. Zool.* **1861**, 16, 5–98.

490 (2) Carnelly, T.; Haldane, J. S.; Anderson, A. M. The carbon acid, organic matter, and micro-
491 organisms in air, more especially of dwellings and schools. *Philos. Transact. R. Soc. Lond.*
492 **B. 1887**, 178, 61–111.

493 (3) Fuzzi, S.; Baltensperger, U.; Carslaw, K.; Decesari, S.; Denier van der Gon, H.; Facchini,
494 M. C.; Fowler, D.; Koren, I.; Langford, B.; Lohmann, U.; Nemitz, E.; Pandis, S.; Riipinen,
495 I.; Rudich, Y.; Schaap, M.; Slowik, J. G.; Spracklen, D. V.; Vignati, E.; Wild,
496 M.; Williams, M.; Gilardoni, S. Particulate matter, air quality and climate: lessons learned
497 and future needs. *Atmos. Chem. Phys.* **2015**, 15, 8217-8299.

498 (4) Després, V. R.; Huffman, J. A.; Burrows, S. M; Hoose, C.; Safatov, A. S.; Buryak, G.;
499 Fröhlich-Nowoisky, J.; Elbert, W.; Andreae, M. O.; Pöschl, U.; Jaenicke, R. Primary
500 biological aerosol particles in the atmosphere: a review. *Tellus B.* **2012**, 64, 15598.

501 (5) Douwes, J.; Thorne, P.; Pearce, N.; Heederik, D. Bioaerosol health effects and exposure
502 assessment: progress and prospects. *Ann. Occup. Hyg.* **2003**, 47, 187–200.

- 503 (6) Hiranuma, N.; Möhler, O.; Yamashita, K.; Tajiri, T.; Saito, A.; Kiselev, A.; Hoffmann, N.;
504 Hoose, C.; Jantsch, E.; Koop, T.; Murakami M. Ice nucleation by cellulose and its
505 potential contribution to ice formation in clouds. *Nature Geosci.* **2015**, 8, 273-277.
- 506 (7) Hader, J. D.; Wright, T. P.; Petters. M. D. Contribution of pollen to atmospheric ice nuclei
507 concentrations *Atmos. Chem. Phys.* **2014**, 14, 5433-5449.
- 508 (8) Gurian-Sherman, D.; Lindow., S. E.; Bacterial ice nucleation: significance and molecular
509 basis. *FASEB J.* **1993**,14, 1338-1343.
- 510 (9) Andreae, M. O.; Rosenfeld, D. Aerosol-cloud-precipitation interactions. Part 1. The nature
511 and sources of cloud-active aerosols. *Earth Sci. Rev.* **2008**, 89, 13–41.
- 512 (10) Ariya, P. A.; Sun, J., Eltouny, N. A.; Hudson, E. D.; Hayes, C. T; Kos, G. Physical and
513 chemical characterization of bioaerosols–implications for nucleation processes. *Int. Rev.*
514 *Phys. Chem.* **2009**, 28, 1–32.
- 515 (11) Andreae, M. O. Aerosols before pollution. *Science.* **2007**, 315, 50-51.
- 516 (12) Fu, P.; Kawamura, K.; Chen, J.; Qin, M.; Ren., L.; Sun, Y.; Wang, Z.; Barrie, L. A.;
517 Tachibana, E.; Ding, A.; Yamashita, Y. Fluorescent water-soluble organic aerosol in the
518 High Arctic atmosphere. *Sci. Rep.* **2015**, 5, 9845.
- 519 (13) Pöhlker, C.; Huffman, J. A.; Pöschl U. Autofluorescence of atmospheric bioaerosols -
520 fluorescent biomolecules and potential interferences. *Atmos. Meas. Tech.*, **2012**, 5, 37–71.
- 521 (14) Chen, Q.; Farmer, D. K.; Schneider, J.; Zorn, S. R.; Heald, C. L; Karl, T. G.; Guenther,
522 A.; Allan, J. D.; Robinson, N.; Coe, H.; Kimmel, J. R.; Pauliquevis, T.; Borrmann, S.;

- 523 Pöschl, U.; Andreae, M. O.; Artaxo, P.; Jimenez, J. L.; Martin, S. T. Mass spectral
524 characterization of submicron biogenic organic particles in the Amazon Basin. *Geophys.*
525 *Res. Lett.* **2009**, 36, L20806.
- 526 (15) Schneider, J.; Freutel, F.; Zorn, S. R.; Chen, Q.; Farmer, D. K.; J. L. Jimenez, Martin, S.
527 T. Artaxo, P.; Wiedensohler, A.; Borrmann, S. Mass-spectrometric identification of
528 primary biological particle markers: indication for low abundance of primary biological
529 material in the pristine submicron aerosol of Amazonia. *Atmos. Chem. Phys. Discuss.*
530 **2011**, 11, 19143–19178.
- 531 (16) Pöschl, U., Martin, S. T., Sinha, B., Chen, Q., Gunthe, S. S.; Huffman, J. A.; Borrmann,
532 S.; Farmer, D.K.; Garland, R. M.; Helas, G.; Jimenez, J. L.; King, S. M.; Manzi, A.;
533 Mikhailov, E.; Pauliquevis, T.; Petters, M. D.; Prenni, A. J.; Roldin, P.; Rose, D.;
534 Schneider, J.; Su, H.; Zorn, S. R.; Artaxo, P.; Andreae, M. O. Rainforest aerosols as
535 biogenic nuclei of clouds and precipitation in the Amazon. *Science*. **2010**, 329, 1513–1516.
- 536 (17) IPCC, 2013: Climate Change 2013: The Physical Science Basis. Contribution of Working
537 Group I to the Fifth Assessment Report of the Intergovernmental Panel on Climate Change
538 [Stocker, T.F.; Qin, D.; Plattner, G.-K.; Tignor, M.; Allen, S. K.; Boschung, J.; Nauels, A.;
539 Xia, Y.; Bex, V.; Midgley, P. M. (eds.)]. Cambridge University Press, Cambridge, United
540 Kingdom and New York, NY, USA, 1535 pp.
- 541 (18) Heald, C. L.; Spracklen D. V. Atmospheric budget of primary biological aerosol particles
542 from fungal spores. *Geophys. Res. Lett.* **2009**, 36, L09806-L09806.

- 543 (19) Bauer, H.; Claeys, M.; Vermeylen, R.; Schueller, E.; Weinke, G.; Berger, A.; Puxbaum,
544 H. Arabitol and mannitol as tracers for the quantification of airborne fungal spores, *Atmos.*
545 *Environ.* **2008**, 42, 588–593.
- 546 (20) Burshtein, N.; Lang-Yona, N.; Rudich, Y. Ergosterol, arabitol and mannitol as tracers for
547 biogenic aerosols in the eastern Mediterranean. *Atmos. Chem. Phys.* **2011**, 11, 829–839.
- 548 (21) Daellenbach, K. R.; Bozzetti, C.; Krepelova, A.; Canonaco, F.; Huang, R.-J.; Wolf, R.;
549 Zotter, P.; Crippa, M.; Slowik, J.; Zhang, Y.; Szidat, S.; Baltensperger, U.; Prévôt, A. S.
550 H.; El Haddad, I. Characterization and source apportionment of organic aerosol using
551 offline aerosol mass spectrometry. *Atmos. Meas. Tech.* **2016**, 9, 23-29.
- 552 (22) Birch, M. E.; Cary, R. A. Elemental carbon-based method for monitoring occupational
553 exposures to particulate diesel exhaust. *Aerosol Sci. and Tech.* **1996**, 25, 221–241.
- 554 (23) Cavalli, F.; Viana, M.; Yttri, K. E.; Genberg, J.; Putaud, J. P. Toward a standardised
555 thermal-optical protocol for measuring atmospheric organic and elemental carbon: the
556 EUSAAR protocol. *Atmos. Meas. Tech.* **2010**, 3, 79-89.
- 557 (24) Piazzalunga, A.; Bernardoni, V.; Fermo, P.; Vecchi, R. Optimisation of analytical
558 procedures for the quantification of ionic and carbonaceous fractions in the atmospheric
559 aerosol and applications to ambient samples. *Anal Bioanal Chem.* **2013**, 405, 1123-32.
- 560 (25) Kunit, M.; Puxbaum, H. Enzymatic determination of the cellulose content of atmospheric
561 aerosols. *Atmos. Environ.* **1996**, 30, 1233-1236.

- 562 (26) Orasche, J.; Schnelle-Kreis, J.; Abbaszade, G.; Zimmermann, R. Technical Note: In-situ
563 derivatization thermal desorption GC-TOFMS for direct analysis of particle-bound non-
564 polar and polar organic species. *Atmos. Chem. Phys.* **2011**, 11, 8977-8993.
- 565 (27) Lang-Yona, N.; Dannemiller, K.; Yamamoto, N.; Burshtein, N.; Peccia, J.; Yarden, O.;
566 Rudich, Y. Annual distribution of allergenic fungal spores in atmospheric particulate
567 matter in the Eastern Mediterranean; a comparative study between ergosterol and
568 quantitative PCR analysis. *Atmos. Chem. Phys.* **2012**, 12, 2681–2690.
- 569 (28) Lang-Yona, N.; Lehahn, Y.; Herut, B.; Burshtein, N.; Rudich, Y. Marine aerosol as a
570 possible source for endotoxins in coastal areas. *Sci. Total Environ.* **2014**, 499, 311–318.
- 571 (29) Yttri, K. E.; Schnelle-Kreis, J.; Maenhaut, W.; Abbaszade, G.; Alves, C.; Bjerke, A.;
572 Bonnier, N.; Bossi, R.; Claeys, M.; Dye, C.; Evtyugina, M.; García-Gacio, D.; Hillamo, R.;
573 Hoffer, A.; Hyder, M.; Iinuma, Y.; Jaffrezo, J.-L.; Kasper-Giebl, A.; Kiss, G.; López-
574 Mahia, P. L.; Pio, C.; Piot, C.; Ramirez-Santa-Cruz, C.; Sciare, J.; Teinilä, K.;
575 Vermeylen, R.; Vicente, A.; Zimmermann, R. An intercomparison study of analytical
576 methods used for quantification of levoglucosan in ambient aerosol filter samples, *Atmos.*
577 *Meas. Tech.*, **2015**, 8, 125-147.
- 578 (30) DeCarlo, P. F.; Kimmel, J. R.; Trimborn, A.; Northway, M. J.; Jayne, J. T.; Aiken, A. C.;
579 Gonin, M.; Fuhrer, K.; Horvath, T.; Docherty, K. S.; Worsnop, D. R.; Jimenez, J. L. Field-
580 deployable, high-resolution, time-of-flight aerosol mass spectrometer. *Anal. Chem.* **2006**,
581 78, 8281–8289.

- 582 (31) Hospodsky, D.; Yamamoto, N.; Peccia, J.; Accuracy, precision, and method detection
583 limits of quantitative PCR for airborne bacteria and fungi. *Appl. Environ. Microb.* **2010**,
584 76, 7004-7012.
- 585 (32) Sundararaj, S.; Guo, A.; Habibi-Nazhad, B.; Rouani, M.; Stothard, P.; Ellison, M.;
586 Wishart, D. S. The CyberCell Database (CCDB): a comprehensive, self-updating,
587 relational database to coordinate and facilitate in silico modeling of *Escherichia coli*.
588 *Nuclei Acid Res.* **2004**, 32, D263-D265.
- 589 (33) Crilley, L. R.; Ayoko, G. A.; Morawska, L. Analysis of organic aerosols collected on
590 filters by Aerosol Mass Spectrometry for source identification. *Anal. Chim. Acta.* **2013**,
591 803, 91– 96.
- 592 (34) Paatero, P.; Tapper, U. Positive matrix factorization - a nonnegative factor model with
593 optimal utilization of error-estimates of data values. *Environmetrics* **1994**, 5, 111-126.
- 594 (35) Ulbrich, I. M.; Canagaratna, M. R.; Cubison, M. J.; Zhang, Q.; Ng, N. L.; Aiken, A. C.;
595 Jimenez, J. L. Three-dimensional factorization of size-resolved organic aerosol mass
596 spectra from Mexico City. *Atmos. Meas. Tech.* **2012**, 5, 195–224.
- 597 (36) Tucker, L. R. Some mathematical notes on 3-mode factor analysis. *Psychometrika* **1966**,
598 31, 279–311.
- 599 (37) Paatero, P.; Hopke, K. Rotational tools for factor analytic models. *J. Chemometr.* **2009**,
600 23, 91–100.
- 601 (38) Canonaco, F.; Crippa, M.; Slowik, J. G.; Baltensperger, U.; Prévôt, A. S. H. SoFi, an
602 IGOR-based interface for the efficient use of the generalized multilinear engine (ME-2) for

603 the source apportionment: ME-2 application to aerosol mass spectrometer data. *Atmos.*
604 *Meas. Tech.* **2013**, 6, 3649-3661.

605 (39) Mohr, C.; DeCarlo, P. F.; Heringa, M. F.; Chirico, R.; Slowik, J. G.; Richter, R.; Reche,
606 C.; Alastuey, A.; Querol, X.; Seco, R.; Penuelas, J.; Jimenez, J. L.; Crippa, M.;
607 Zimmermann, R.; Baltensperger, U.; Prevot, A. S. H. Identification and quantification of
608 organic aerosol from cooking and other sources in Barcelona using aerosol mass
609 spectrometer data. *Atmos. Chem. Phys.* **2012**, 12, 1649-1665.

610 (40) Aiken, A. C.; DeCarlo, P. F.; Kroll, J. H.; Worsnop, D. R.; Huffmann, J. A.; Docherty, K.
611 S.; Ulbrich, I. M.; Mohr, C.; Kimmel, J. R.; Sueper, D.; Sun, Y.; Zhang, Q.; Trimborn, A.;
612 Northway, M.; Ziemann, P. J.; Canagaratna, M. R.; Onasch, T. B.; Alfarra, M. R.; Prevot,
613 A. S. H.; Dommen, J.; Duplissy, J.; Metzger, A.; Baltensperger, U.; Jimenez J. L. O/C and
614 OM/OC ratios of primary, secondary, and ambient organic aerosols with high-resolution
615 time-of-flight aerosol mass spectrometry. *Environ. Sci. Technol.*, **2008**, 42, 4478-4485.

616 (41) Allan, J. D.; Jimenez, J. L.; Williams, P. I.; Alfarra, M. R.; Bower, K. N.; Jayne, J. T.;
617 Coe, H.; Worsnop, D. R. Quantitative sampling using an Aerodyne aerosol mass
618 spectrometer 1. Techniques of data interpretation and error analysis. *J. Geophys. Res.*,
619 **2003**, 108 (D3), 4090.

620 (42) Ulbrich, I. M.; Canagaratna, M. R.; Zhang, Q.; Worsnop, D. R.; Jimenez, J. L.
621 Interpretation of organic components from positive matrix factorization of aerosol mass
622 spectrometric data. *Atmos. Chem. Phys.* **2009**, 9, 2891-2918.

623 (43) Crippa, M.; Canonaco, F.; Slowik, J. G.; El Haddad, I.; DeCarlo, P. F.; Mohr, C.;
624 Heringa, M. F.; Chirico, R.; Marchand, N.; Temime-Roussel, B.; Abidi, E.; Poulain,

625 L.; Wiedensohler, A.; Baltensperger, U.; Prévôt, A. S. H. Primary and secondary organic
626 aerosol origin by combined gas-particle phase source apportionment. *Atmos. Chem. Phys.*
627 **2013**, 13, 8411-8426.

628 (44) Barmapadimos, I.; Nufer, M.; Oderbolz, D. C.; Keller, J.; Aksoyoglu, S.; Hueglin, C.;
629 Baltensperger, U.; Prevot A. S. H. The weekly cycle of ambient concentrations and traffic
630 emissions of coarse (PM(10)-PM(2.5)) atmospheric particles, *Atmos. Environ.* **2011**, 45,
631 4580-4590.

632 (45) Chow, J.; Watson, J.; Ashbaugh, L. L.; Magliano, K. L. Similarities and differences in
633 PM10 chemical source profiles for geological dust from the San Joaquin Valley, California.
634 *Atmos. Environ.* **2003**, 37, 1317-1340.

635 (46) Amato, F.; Pandolfia, M.; Moreno, T.; Furger, M.; Pey, J.; Alastuey, A.; Bukowiecki, N.;
636 Prevot, A.S.H.; Baltensperger, U.; Querol X. Sources and variability of inhalable road dust
637 particles in three European cities. *Atmos. Environ.* **2011**, 45, 6777-6787.

638 (47) El Haddad, I.; Marchand, N.; Drona, J.; Temime-Roussel, B.; Quivet, E.; Wortham, H.;
639 Jaffrezo, J.-L.; Baduel, C.; Voisin, D.; Besombes, J. L.; Gille, G. Comprehensive primary
640 particulate organic characterization of vehicular exhaust emissions in France. *Atmos.*
641 *Environ.* **2009**, 43, 6190-6198.

642 (48) Huang, R.-J.; Zhang, Y.; Bozzetti, C.; Ho, K.-F.; Cao, J.; Han, Y.; Dällenbach, K. R.;
643 Slowik, J. G.; Platt, S. M.; Canonaco, F.; Zotter, P.; Wolf, R.; Pieber, S. M.; Bruns, E. A.;
644 Crippa, M.; Ciarelli, G.; Piazzalunga, A.; Schwikowski, M.; Abbaszade, G.; Schnelle-
645 Kreis, J.; Zimmermann, R.; An, Z.; Szidat, S.; Baltensperger, U.; El Haddad, I.; Prévôt, A.

- 646 S. H. High secondary aerosol contribution to particulate pollution during haze events in
647 China, *Nature*. **2014**, 514, 218-212.
- 648 (49) Canonaco, F.; Slowik, J. G.; Baltensperger, U.; Prévôt, A. S. H. Seasonal differences in
649 oxygenated organic aerosol composition: implications for emissions sources and factor
650 analysis. *Atmos. Chem. Phys.* **2015**, 15, 6993-7002.
- 651 (50) Crippa, M.; Canonaco, F.; Lanz, V. A.; Äijälä, M.; Allan, J. D.; Carbone, S.; Capes, G.;
652 Ceburnis, D.; Dall'Osto, M.; Day, D. A.; DeCarlo, P. F.; Ehn, M.; Eriksson, A.; Freney, E.;
653 Hildebrandt Ruiz, L.; Hillamo, R.; Jimenez, J. L.; Junninen, H.; Kiendler-Scharr, A.;
654 Kortelainen, A.- M.; Kulmala, M.; Laaksonen, A.; Mensah, A. A.; Mohr, C.; Nemitz, E.;
655 O'Dowd, C.; Ovadnevaite, J.; Pandis, S. N.; Petäjä, T.; Poulain, L.; Saarikoski, S.; Sellegri,
656 K.; Swietlicki, E.; Tiitta, P.; Worsnop, D. R.; Baltensperger, U.; Prévôt, A. S. H. Organic
657 aerosol components derived from 25 AMS data sets across Europe using a consistent ME-2
658 based source apportionment approach. *Atmos. Chem. Phys.* **2014**, 14, 6159–6176.
- 659 (51) Medeiros, P. M.; Conte, M. H.; Weber, J. C.; Simoneit, B. R. T. Sugars as source
660 indicators of biogenic organic carbon in aerosols collected above the Howland
661 Experimental Forest, Maine. *Atmos. Environ.* **2006**, 40, 1694-1705.
- 662 (52) Jia, Y.; Clements, A. L.; Fraser, M. P. Saccharide composition in atmospheric particulate
663 matter in the southwest US and estimates of source contributions. *J. Aerosol Sci.* **2010**, 41,
664 62-73.
- 665 (53) Williams, L. R.; Gonzalez, L. A.; Peck, J.; Trimborn, D.; McInnis, J.; Farrar, M. R.;
666 Moore, K. D.; Jayne, J. T.; Robinson, W. A.; Lewis, D. K.; Onasch, T. B.; Canagaratna, M.
667 R.; Trimborn, A.; Timko, M. T.; Magoon, G.; Deng, R.; Tang, D.; de la Rosa Blanco, E.;

- 668 Prévôt, A. S. H.; Smith, K. A.; Worsnop D. Characterization of an aerodynamic lens for
669 transmitting particles greater than 1 micrometer in diameter into the Aerodyne aerosol mass
670 spectrometer. *Atmos. Meas. Tech.* **2013**, 6, 3271–3280.
- 671 (54) Rogge, W. F.; Hildemann, L. M.; Mazurek, M. A.; Cass, G. R.; Simoneit, B. R. T.
672 Sources of fine organic aerosol. 4. Particulate abrasion products from leaf surfaces of urban
673 plants, *Environ. Sci. Technol.*, **1993**, 27 (13), 2700–2711.
- 674 (55) Kotianová, P.; Puxbaum, H.; Bauer, H.; Caseiro, A.; Marrb, I. L.; Čìk, G.; Temporal
675 patterns of n-alkanes at traffic exposed and suburban sites in Vienna. *Atmos. Environ.*
676 **2008**, 42, 2993–3005.
- 677 (56) Rogge, W. F.; Hildemann, L. M.; Mazurek, M.,A.; Caw, G. R. Sources of Fine Organic
678 Aerosol. 2. Noncatalyst and Catalyst-Equipped Automobiles and Heavy-Duty Diesel
679 Trucks. *Environ. Sci. Technol.* **1993**, 27, 636-651.
- 680 (57) Hildemann, L. M.; Mazurek, M. A.; Cass, G. R.; Simoneit, B. R. Quantitative
681 characterization of urban sources of organic aerosol by high-resolution gas-
682 chromatography, *Environ. Sci. Technol.* **1991**, 25, 1311-1325.
- 683 (58) Borodulin, A.; Safatov, A.; Belan, B.; Panchenko, M. Measurement errors in determining
684 tropospheric bioaerosol concentrations in the southern region of Western Siberia. *Dokl.*
685 *Biol. Sci.* **2005**, 403, 260–262.
- 686 (59) Vlodayets, V.; Mats, L. The influence of meteorological factors on the microflora of the
687 atmospheric air in Moscow. *J. Microbiol.* **1958**, 59, 539–544.

688 (60) Pady, S.; Kelly, C. Aerobiological studies of fungi and bacteria over the Atlantic Ocean.
689 Can. J. Botany. **1954**, 32, 202–212.

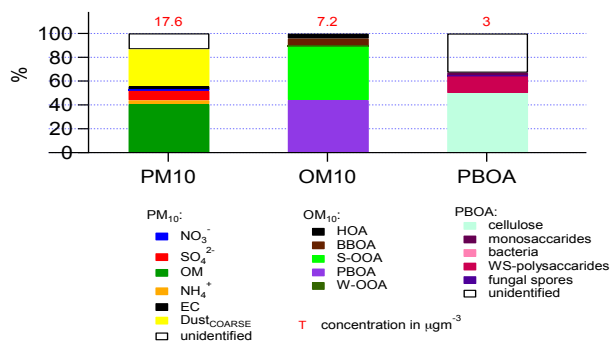
690 (61) Burrows, S. M.; Elbert, W.; Lawrence, M. G.; Pöschl, U. Bacteria in the global
691 atmosphere–Part 1: Review and synthesis of literature data for different ecosystems.
692 Atmos. Chem. Phys. **2009**, 9, 9281–9297.

693 (62) El Haddad, I.; D'Anna, B.; Temime-Roussel, B.; Nicolas, M.; Boreave, A.; Favez, O.;
694 Voisin, D.; Sciare, J.; George, C.; Jaffrezo, J.-L.; Wortham, H.; Marchand, N.
695 Towards a better understanding of the origins, chemical composition and aging of
696 oxygenated organic aerosols: case study of a Mediterranean industrialized environment,
697 Marseille. Atmos. Chem. Phys. **2013**, 13, 7875-7894.

698

699

700 Graphical TOC Entry



701